NASA CR-175,610

NASA-CR-175670
19850015392

A Reproduced Copy

OF

NASA CR-175,670

Reproduced for NASA

by the

NASA Scientific and Technical Information Facility

FFNo 672 Aug 65

SEMI-ANNUAL STATUS REPORT

November 1984 - April 1985

for NASA Grant NSG 1419

THE STRUCTURE OF SEPARATED FLOW REGIONS OCCURRING NEAR THE LEADING EDGE OF AIRFOILS - INCLUDING TRANSITION

Thomas J. Mueller
Principal Investigator

Department of Aerospace and Mechanical Engineering
University of Notre Dame
Notre Dame, Indiana 46556

April 1985

Semi-Annual Status Report
November 1984 -April 1985
NSG 1419*

All of the time and effort during this report period was directed toward acquiring, reducing and analyzing hot-wire anemometer data. This experimental study included twelve combinations of chord Reynolds number, angle of attack, and freestream disturbance environment using the NACA 66_3-018 airfoil.

This research has as its objective the detailed documentation of the structure and behavior of the separation bubble including transition and the redeveloping boundary layer after reattachment over an airfoil at low Reynolds numbers. The intent of this work is to further the understanding of the complex flow phenomena so that analytic methods for predicting their formation and development can be improved. These analytic techniques have applications in the design and performance prediction of airfoils operating in the low Reynolds number flight regime.

CALCULATION OF PARAMETERS

The primary results of this investigation are the various flow field parameters that were calculated from the basic data. A majority of these parameters were local variables calculated at the points of separation, transition, and reattachment. Since the locations of these points were altered slightly as additional data was taken, a computer code was developed to handle the large number of tedious calculations. Although this calculation scheme was generic in nature, the vast similarities that existed in the data allowed for accurate and consistent computation of the parameters. Some precautions had to be taken however, and these will be discussed in more detail.

---

* NASA Technical Monitor for this Grant is
Mr. Dan M. Somers, NASA Langley Research Center,
Hampton, Virginia 23665.

Most of the parameters included in Tables I and II are derived from the basic boundary layer variables and require little additional discussion once the definition is provided. The definitions of the parameters can be found in the list of nomenclature or on Figure 1. In the case of the two angular parameters, however, further discussion of the definition and calculation technique is required.

Separation Bubble Locations

Before any parameters could be calculated, the locations of flow separation, transition, and reattachment had to be determined. These important locations, which collectively describe the basic character of all laminar separation bubbles, were determined through a careful examination of the static pressure and hot-wire anemometry data. Since static pressure data was available at closer intervals along the airfoil upper surface, it was used as the primary indicator of bubble locations. The hot-wire profiles were used to confirm the pressure data, and in the case of separation, were sometimes used to further pinpoint the actual location. In general, the pressure and hot-wire data showed good agreement, and together provided sufficient information for determining detailed bubble locations.

In order to determine separation, transition, and reattachment locations in a consistent manner, it was sometimes necessary to choose locations between adjacent pressure taps. In the case of separation, this type of location would later permit accurate calculation of the local pressure and velocity gradients. The locations of transition and reattachment were taken as those points at which the pressure distribution exhibited sharp discontinuities. These discontinuities were sometimes masked because of the finite distances between taps. Thus, interpolation between points was necessary to simulate the linear pressure increase that usually exists between transition and

reattachment. In general, this process allowed for greater consistency in locating the various flow phenomena associated with the separation bubble.

Further justification for assigning locations between taps came from the need for defining uncertainty bands. In most cases, it was obvious that the important bubble locations occurred between a pair of adjacent pressure taps. When this occurred, central locations between the taps were chosen so that uncertainty bands extending across the two taps could be established. Although the exact locations of these various flow phenomena can be disputed to some degree, the locations determined represent mean positions within the bands of uncertainty. These uncertainties only apply to the pressure distributions obtained in this investigation which were shown to be very repeatable. Long term repeatibility tests, however, might reveal slight deviations which would further extend the uncertainty bands. In general, small variations in separation, transition, and reattachment locations did not significantly affect the final results. The bubble locations associated with each of the experimental cases are summarized in Table III.

Application of Definitions

Although the definitions of the various flowfield parameters are relatively straightforward, their application to a discrete set of data is not necessarily trivial. On an airfoil, for example, all length dimensions should be measured along the curved surface. The origin of this coordinate is usually taken as the point of flow stagnation. In this investigation, the arc lengths along the airfoil surface were approximated by summing the line segment contributions calculated from the coordinate points. Fortunately, additional coordinate points were available near the leading edge so that the linear approximation was very good.

Another potential problem arose in choosing suitable values of the

external velocities. Because of the effects of hot-wire probe orientation, the pressure data was used to obtain all external velocity magnitudes. Since the locations of separation and transition, as determined by the process described above, sometimes fell on gradient regions of the pressure distributions, the associated external velocities were measured at the extreme ends of the pressure plateaus instead of at the actual locations. Although a relatively minor point, this distinction was necessary to combine the effects of consistent bubble locations with accurate parameter calculations.

Because it was necessary to survey the entire boundary layer over the airfoil, it was not possible to take data at close enough intervals to always correspond to the exact locations of separation, transition, and reattachment. For this reason, an interpolation scheme was employed to calculate values at the points of interest. To determine the integrated thicknesses at separation, for example, it was sometimes necessary to interpolate between an upstream and a downstream value. Fortunately, in most cases, data was available at stations at or very near the desired location so that the resultant interpolated values were very reliable.

Definition of Angular Parameters

The turbulent spreading angle α_T is a parameter suggested by the simplified bubble model shown in Figure 1. In attempting to approximate the magnitude of this angle, the geometric simplification shown in Figure 2a was employed. Here, the "origin" of the turbulence was taken to be the point of maximum turbulence intensity at transition. This point generally fell at or very near the vertical center of the free shear layer. From this point, the turbulence was assumed to spread between two linear boundaries extending outward to the boundary layer edge and the airfoil surface at reattachment. With this simplification, calculation of α_T became trivial once the points of

transition and reattachment were determined.

The final parameter which requires additional discussion is the angle γ formed between the airfoil surface and the separation streamline. Because of the problems associated with the flow visualization data, a direct measurement of this angle was basically impossible. As such, it was necessary to use hot-wire velocity profiles to estimate this important parameter. This procedure involved determining the heights of the recirculation region at three or more stations just downstream of separation. These heights were defined as those distances over which the velocity ratios U/U_{fs} were very small, and the profiles had extremely large slopes. These heights were plotted versus the surface arc length at which the corresponding profiles were taken. This particular definition of a separation angle on a curved surface is similar to that proposed by Dobbinga et al [1]. Fortunately, the points corresponding to the laminar free shear layer generally fell on a single line which could be extrapolated back to form an angle. The separation angle so defined is shown schematically in Figure 2b.

DISCUSSION OF RESULTS

During the data acquisition phase of this investigation, the separation bubble flowfield over the airfoil was surveyed for twelve different conditions. These conditions were chosen in such a way that the effects of Reynolds number, angle of attack, and disturbance environment could be isolated. Along with indicating such behavioral trends, the data also provided valuable insight into the structure of the separation bubble. In addition, the development of the turbulent boundary layer downstream of reattachment was investigated.

The important separation bubble parameters are compiled together in Tables I and II. These values were calculated from the basic data once the

positions of separation, transition, and reattachment were determined. A list of the actual bubble locations used in the analysis is included in Table III. As illustrated in Figure 1, the length dimensions, l_1, l_2, and l_B used throughout this investigation represent distances measured along the airfoil surface. Definitions of the various parameters are included in the list of nomenclature. The more involved calculation schemes used to determine the angular parameters α_T and γ were described earlier.

General Separation Bubble Characteristics

As shown in Figures 3 and 4, the chord Reynolds number has an important effect on the separation bubble flowfield. These figures show the effects of Reynolds number for the one and zero flow restrictor cases respectively. As Figure 3 indicates, the length of the separation bubble decreases as the chord Reynolds number is increased. As the tunnel speed is elevated to achieve higher Reynolds number testing conditions, the rate at which small disturbances are being amplified in the unstable laminar shear layer is increased. This causes forward movement in the point of transition which subsequently reduces the overall length of the separation bubble.

As the bubble diminishes in length, the pressure distribution becomes less "distorted", and a higher suction peak is attained. This implies that changes in the separation bubble significantly affect the entire leading edge flow. As a result, the upstream pressure distribution is highly dependent on the chord Reynolds number. As shown in Figure 4, however, the effect of the bubble on the downstream flowfield appears to be minimal.

The effect of chord Reynolds number on total bubble length is summarized in Figure 5. In this figure, the bubble lengths l_B listed in Table I are plotted versus Reynolds number for all of the 12 degree angle of attack cases. As indicated, the bubble more than doubles in length as the chord Reynolds

number is decreased from R_c = 140,000 to R_c = 50,000. Each of the different flow restrictor cases exhibit the same trend with Reynolds number although the magnitudes of l_B are shifted. This can be seen by the dotted line which connects the three cases at R_c = 140,000. The shift in magnitude of l_B indicates that bubble length is also a direct function of the disturbance environment. Although the level of freestream turbulence increased as the chord Reynolds number (tunnel speed) was increased, the latter effect appears to predominate. It is, however, impossible to totally uncouple the two effects when changes in tunnel speed are used to alter the chord Reynolds number.

Although changes in Reynolds number could not be achieved without slight changes in the disturbance environment for the given model, it was possible to isolate the effects of freestream turbulence. This was made possible through the introduction of flow restrictors which have been shown to alter the testing environment [2]. Pressure distributions obtained at various levels of freestream turbulence are shown in Figures 6 and 7. As the turbulence level is increased, the bubble is reduced in length, and the suction peak grows in absolute magnitude. This well known phenomenon so closely resembles those effect obtained by increasing the chord Reynolds number that the two are often equated. This has given rise to the use of "effective" Reynolds numbers when dealing with various disturbance environments or when discussing the effects of different types of surface roughness [3].

The correlation between increases in freestream turbulence and increases in Reynolds number is shown dramatically in Figure 8. Except for the slight deviation in the suction peaks, these distributions are basically identical. Thus, the case of R_c = 140,000, α = 12°, 2 flow restrictors can be said to have an "effective" chord Reynolds number of 200,000 with 0 flow restrictors.

Starting from the base condition (R_c = 140,000, OFR), an increase in turbulence intensity of 612% or an increase in Reynolds number of 43% is required to produce the common pressure distribution. Associated with the Reynolds number increase was a 42% increase in the freestream turbulence intensity. Given these incremental magnitudes, it appears that, in general, the small rise in turbulence level associated with increases in tunnel speed contributes relatively little to the overall effect of increasing the chord Reynolds number. Thus, for a given tunnel configuration, changes in speed predominate over accompanying changes in turbulence levels as the driving mechanism which affects the separation bubble.

Along with chord Reynolds number and freestream turbulence intensity, the separation bubble flowfield is also affected by changes in angle of attack. These effects are shown in Figures 9-11 for three different testing conditions. As the angle of attack is increased from 8 to 10 degrees, the point of laminar separation moves forward from approximately 3.7% to approximately 2.8% X/C, but there is no significant change in the length of the bubble. At 12 degrees angle of attack, the bubble has again moved forward but has now increased in length. As a given angle of attack, the separation point reamins essentially unchanged over the entire range of Reynolds number. The effect of angle of attack on the bubble length l_b is summarized in Figure 12.

In addition to the overall length, the thickness of the separation bubble is a parameter that is significantly affected by the various testing conditions. For the sake of comparision, the height of the recirculation region at transition $(H_B)_T$ was determined from each set of velocity profiles. These thicknesses are plotted versus chord Reynolds number in Figure 13. This figure indicates that a sharp reduction in bubble thickness occurs as the

chord Reynolds number is increased. The bubble at R_c = 50,000 is almost 3 times thicker at transition than the corresponding bubble at R_c = 140,000. This seems to imply that the bubble thickness is closely related to the total bubble length. This almost linear relationship is plotted in Figure 14. The limited number of points available in Table I also indicate that the bubble thickness increases as the angle of attack is increased. This phenomenon was confirmed by flow visualization data.

In addition to determining the overall separation bubble characteristics, the recent work has focused on documenting the various structural components comprising the bubble. This documentation involved a detailed investigation of the various flow phenomena associated with the bubble, as well as, a study of the redeveloping turbulent boundary layer downstream of reattachment. Once this documentation was completed, the large amount of experimental data was analyzed in terms of existing physical and mathematical models of the flow field. The results of this analysis indicated that further work is needed to adequately model the flow over an airfoil at low Reynolds numbers. It appears, however, that this work, which is described in detail in Reference [2], has provided the groundwork for future improvements in the design and performance prediction of low Reynolds number airfoils.

During this report period the following publications were written and/or published under this grant:

Mueller, T.J., "The Influence of Laminar Separation and Transition on Low Reynolds Number Airfoil Hysteresis," AIAA 17th Fluid Dynamics, Plasma Dynamics, and Lasers Conference, Snowmass, Colorado, June 25-27, 1984, (accepted for publication in AIAA Journal of Aircraft).

O'Meara, M.M., "An Experimental Investigation of the Separation Bubble Flow Field Over an Airfoil at Low Reynolds Numbers," M.S. Thesis, University of Notre Dame, 1985.

O'Meara, M.M., Schmidt, G.S., and Mueller, T.J., "Experimental Studies of the Laminar Separation Bubble," Proceedings of the Conference on Low Reynolds Number Airfoil Aerodynamics, University of Notre Dame, June 1985

REFERENCES

1. Dobbinga, E., vanIngen, J.L., and Kocf, J.W., "Some Research on Two-Dimensional Laminar Separation Bubbles," Technological University of Delft, Kluyverweg 1, Delft, The Netherlands.

2. O'Meara, M.M., "An Experimental Investigation of the Separation Bubble Flow Field Over an Airfoil at Low Reynolds Numbers," M.S. Thesis, University of Notre Dame, 1985.

3. Huber III, A.F., "The Effects of Roughness on an Airfoil at Low Reynolds Numbers," M.S. Thesis, University of Notre Dame, 1985.

NOMENCLATURE

C	Airfoil chord, mm
C_p	Pressure coefficient, $C_p = (P_l - P_{fs})/Q_{fs}$
FR	Flow Restrictor
H_T	Transition height, mm
H_{12}	Shape factor equal to the boundary layer displacement thickness divided by the momentum thickness
H_{32}	Shape factor equal to the boundary layer energy thickness divided by the momentum thickness
ℓ_B	Total bubble length, mm
ℓ_1	Bubble length from separation to transition
ℓ_2	Bubble length from transition to reattachment
R_{δ_2}	Reynolds number based on momentum thickness, $U \delta_2 \rho/\mu$
R_{l_1}	Reynolds number based on laminar length, $U l_1 \rho/\mu$
R	Reattachment location
R_{δ_1}	Reynolds number based on displacement thickness, $U \delta_1 \rho/\mu$
R_C	Chord Reynolds number
R_S	Reynolds number based on surface arc length
R_{l_B}	Reynolds number based on total bubble length
S	Laminar separation location - Surface arc length coordinate
S'	Turbulent separation location
T	Location of approximate end of transition
U	Velocity
U'	Fluctuating velocity component
U_{fs}	Freestream velocity
X/C	Nondimensional distance along chord

Greek Symbols

α	Angle of attack
γ	Separation angle
α_T	Turbulent spreading angle
δ_1	Boundary layer displacement thickness
δ_3	Boundary layer energy thickness
δ_2	Boundary layer momentum thickness
ν	Kinematic viscosity
ρ	Density

Subscripts

fs	Freestream
R	Reattachment
S	Separation
T	Transition
ext	External
atm	Atmosphere
w	Uncertainty magnitude
B	Bubble
S'	Turbulent Separation

TABLE I

IMPORTANT FLOW FIELD PARAMETERS

Parameter \ Condition	R_c=140K α=12° 0FR	R_c=160K α=12° 0FR	R_c=200K α=12° 0FR	R_c=50K α=12° 1FR	R_c=80K α=10° 1FR	R_c=80K α=12° 1FR	R_c=100K α=10° 1FR	R_c=100K α=12° 1FR	R_c=140K α=12° 1FR	R_c=50K α=10° 2FR	R_c=50K α=12° 2FR	R_c=140K α=12° 2FR
ϵ_B (S/C %)	13.6	12.3	9.0	22.0	12.7	16.7	10.2	14.2	10.3	15.5	18.8	9.0
ϵ_1 (S/C %)	7.1	6.4	4.8	12.9	8.3	9.2	6.9	7.8	5.5	10.0	11.0	4.8
ϵ_2 (S/C %)	6.5	5.9	4.2	9.1	4.4	7.5	3.3	6.4	4.9	5.5	7.8	4.2
$(H_B)_T$ (%C)	0.54	0.46	0.29	1.13	0.54	0.80	0.42	0.63	0.37	0.67	1.13	0.33
H_T (% C)	0.79	0.64	0.46	1.69	0.77	1.29	0.67	0.82	0.63	0.86	1.29	0.54
U_S (m/s)	17.0	19.9	25.6	5.7	9.2	9.4	11.7	12.0	17.3	5.7	5.9	17.9
U_T (m/s)	17.1	20.0	25.4	5.6	9.2	9.4	11.7	12.1	17.2	5.7	5.8	17.9
U_R (m/s)	13.5	15.5	20.3	4.5	7.4	7.5	9.5	9.5	13.5	4.6	4.6	14.0
$(\delta_1)_S$ (%C)	0.16	0.18	0.14	0.25	0.23	0.24	0.19	0.23	0.19	0.26	0.25	0.17
$(\delta_1)_R$ (%C)	0.63	0.66	0.35	1.37	0.45	0.90	0.41	0.75	0.44	0.91	1.34	0.41
$(\delta_2)_S$ (%C)	0.040	0.034	0.036	0.059	0.059	0.050	0.052	0.043	0.044	0.079	0.073	0.040
$(\delta_2)_R$ (%C)	0.36	0.37	0.20	0.65	0.25	0.48	0.23	0.39	0.26	0.35	0.60	0.23
$(H_{12})_S$	4.09	4.66	3.88	4.16	3.90	4.48	3.50	4.91	4.28	3.26	3.38	4.20
$(H_{12})_R$	1.75	1.78	1.72	2.08	1.82	1.88	1.75	1.94	1.71	2.30	2.25	1.75

TABLE II

IMPORTANT FLOW FIELD PARAMETERS CONT'D

Parameter \ Condition	R_c=140K α=12° OFR	R_c=160K α=12° OFR	R_c=200K α=12° OFR	R_c=50K α=12° IFR	R_c=80K α=10° IFR	R_c=80K α=12° IFR	R_c=100K α=10° IFR	R_c=100K α=12° IFR	R_c=140K α=12° IFR	R_c=50K α=10° 2FR	R_c=50K α=12° 2FR	R_c=140K α=12° 2FR
$(H_{32})_S$	1.49	1.57	1.51	1.52	1.53	1.54	1.51	1.48	1.50	1.50	1.53	1.50
$(H_{32})_R$	1.65	1.64	1.66	1.56	1.63	1.61	1.66	1.61	1.66	1.55	1.57	1.65
$R_{\ell B} \times 10^{-4}$	3.71	3.85	3.76	2.05	1.88	2.42	1.86	2.64	2.80	1.40	1.73	2.54
$R_{\ell 1} \times 10^{-4}$	1.95	2.01	2.03	1.20	1.23	1.34	1.26	1.44	1.48	0.903	1.01	1.37
$(R_S)_S \times 10^{-4}$	1.92	2.20	3.04	0.656	1.00	1.02	1.24	1.31	1.97	0.671	0.699	2.05
$(R_S)_T \times 10^{-4}$	3.07	4.21	5.06	1.86	2.23	2.36	2.50	2.75	3.46	1.57	1.71	3.47
$(R_{\ell 1})_S$	445.0	557.0	589.0	229.0	346.0	343.0	346.0	424.0	514.0	233.0	226.0	489.0
$(R_{S2})_S$	109.0	105.0	150.0	55.0	87.0	72.0	96.0	79.0	119.0	71.0	67.0	113.0
α_T (Deg)	29.0	25.5	27.5	35.5	30.0	26.5	51.0	28.0	25.5	30.5	35.5	26.5
γ (Deg)	8.0	6.5	6.0	9.0	4.0	6.5	5.0	6.5	6.0	3.0	6.5	5.0
$(H_{12})_S^*$	2.56	2.79	2.69	1.87	2.40	2.10	2.52	2.31	2.73	2.68	2.51	2.74
$(H_{32})_S^*$	1.53	1.52	1.53	1.63	1.55	1.58	1.54	1.56	1.52	1.54	1.53	1.52

TABLE III

SEPARATION BUBBLE LOCATIONS

Condition	Separation (X/C %)	Transition (X/C %)	Reattachment (X/C %)
R_c=140,000 Alpha=12 Deg 0 FR	2.0 +/- 0.4	8.7 +/- 0.6	15.0 +/- 1.0
R_c=160,000 Alpha=12 Deg 0 FR	2.0 +/- 0.4	8.0 +/- 0.7	13.7 +/- 1.0
R_c=200,000 Alpha=12 Deg 0 FR	2.2 +/- 0.2	6.7 +/- 0.6	10.7 +/- 0.8
R_c=50,000 Alpha=12 Deg 1 FR	2.0 +/- 0.4	14.3 +/- 0.6	23.3 +/- 1.2
R_c=80,000 Alpha=10 Deg 1 FR	2.8 +/- 0.5	10.7 +/- 0.8	15.0 +/- 0.7
R_c=80,000 Alpha=12 Deg 1 FR	2.0 +/- 0.4	10.7 +/- 0.8	18.0 +/- 1.2
R_c=100,000 Alpha=10 Deg 1 FR	2.8 +/- 0.5	9.3 +/- 0.6	12.5 +/- 0.6
R_c=100,000 Alpha=12 Deg 1 FR	2.0 +/- 0.4	9.3 +/- 0.6	15.6 +/- 1.2
R_c=140,000 Alpha=12 Deg 1 FR	2.2 +/- 0.2	7.3 +/- 0.4	12.0 +/- 0.5
R_c=50,000 Alpha=10 Deg 2 FR	3.4 +/- 0.4	13.0 +/- 0.5	18.4 +/- 1.2
R_c=50,000 Alpha=12 Deg 2 FR	2.5 +/- 0.3	13.0 +/- 0.5	20.7 +/- 1.2
R_c=140,000 Alpha= 12 Deg 2 FR	2.2 +/- 0.2	6.7 +/- 0.6	10.7 +/- 0.8

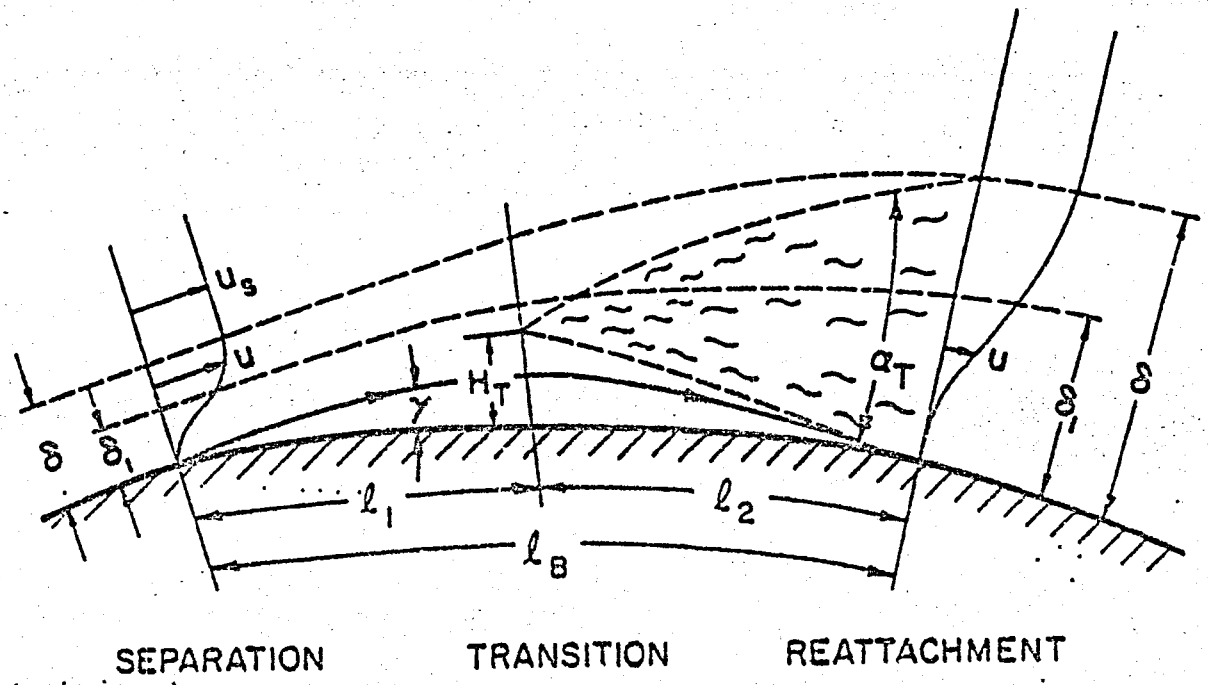

Figure 1. Two-Dimensional Separation Bubble Model Suggested by Eppler

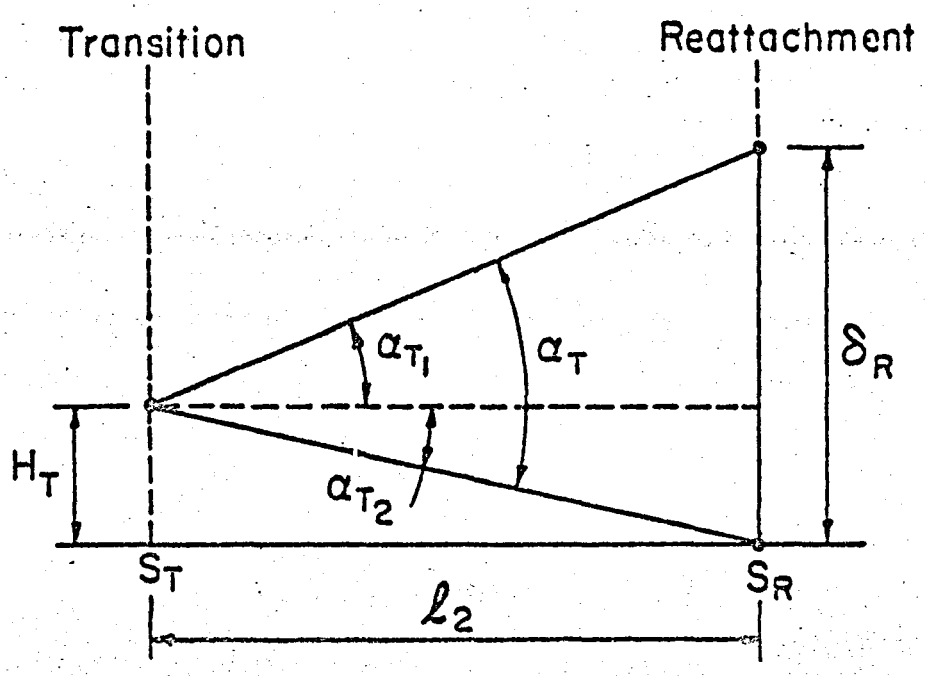

a. Turbulent Spreading Angle

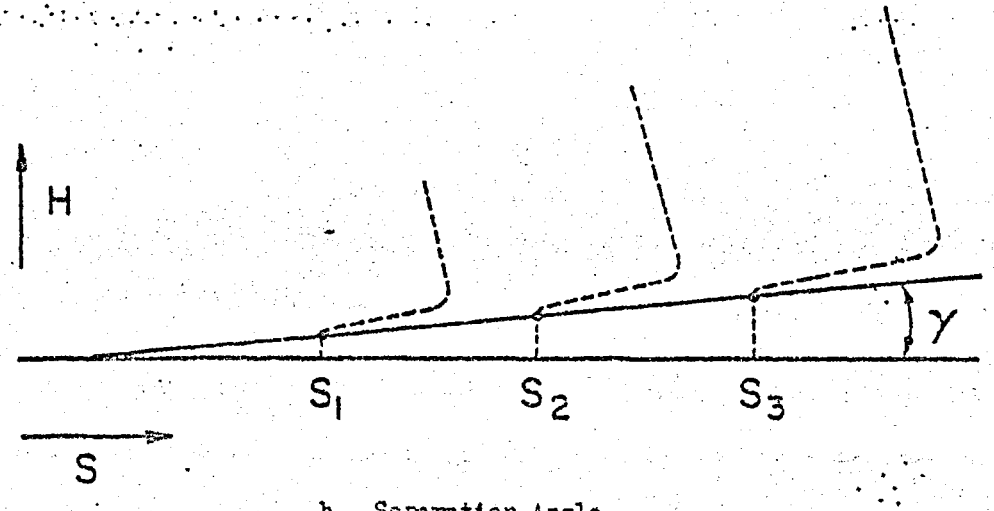

b. Separation Angle

Figure 2. Calculation Techniques for Angular Parameters

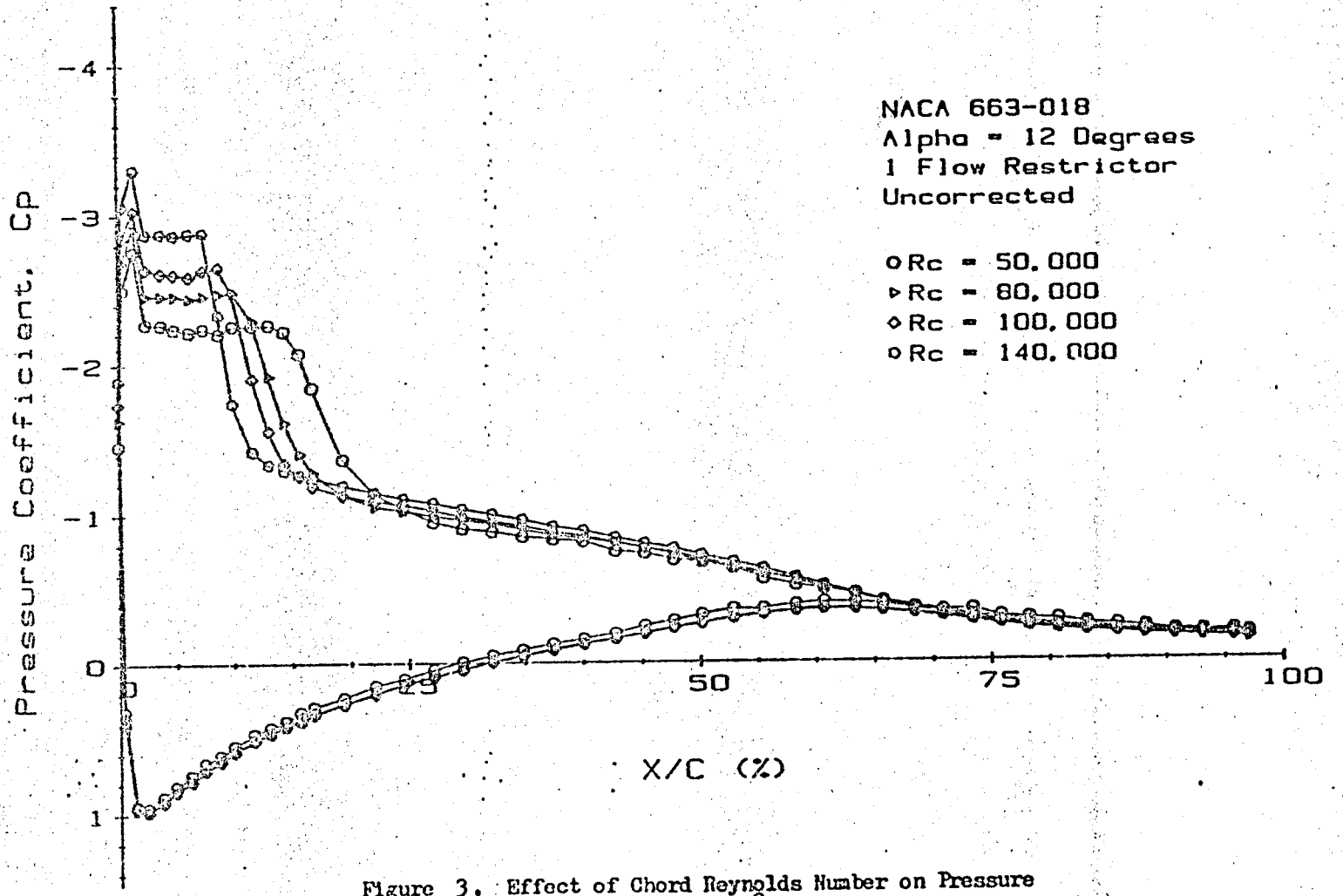

Figure 3. Effect of Chord Reynolds Number on Pressure Distribution, $\alpha = 12^{\circ}$, 1 Flow Restrictor

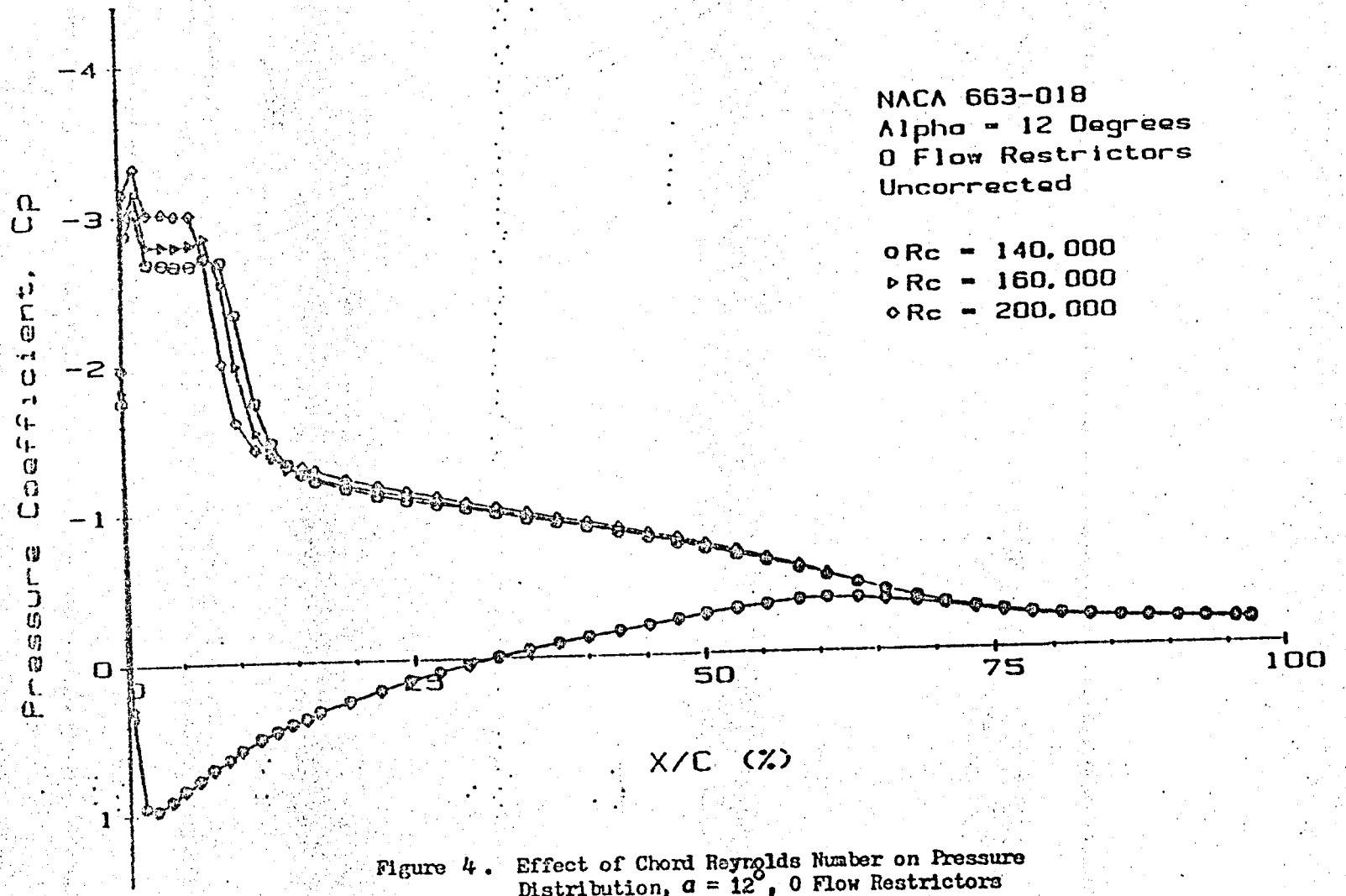

Figure 4. Effect of Chord Reynolds Number on Pressure Distribution, $\alpha = 12^{\circ}$, 0 Flow Restrictors

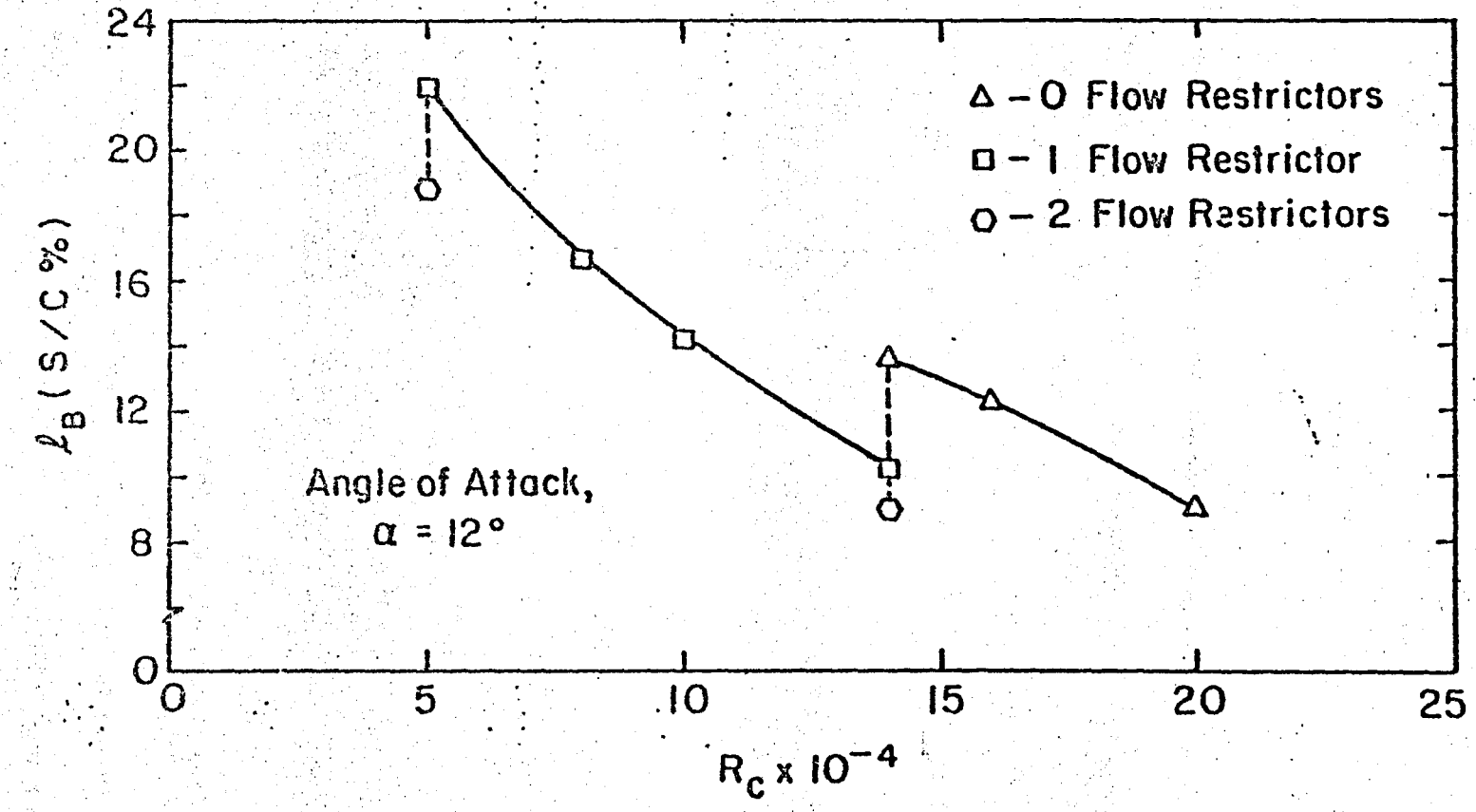

Figure 5. Total Bubble Length versus Chord Reynolds Number

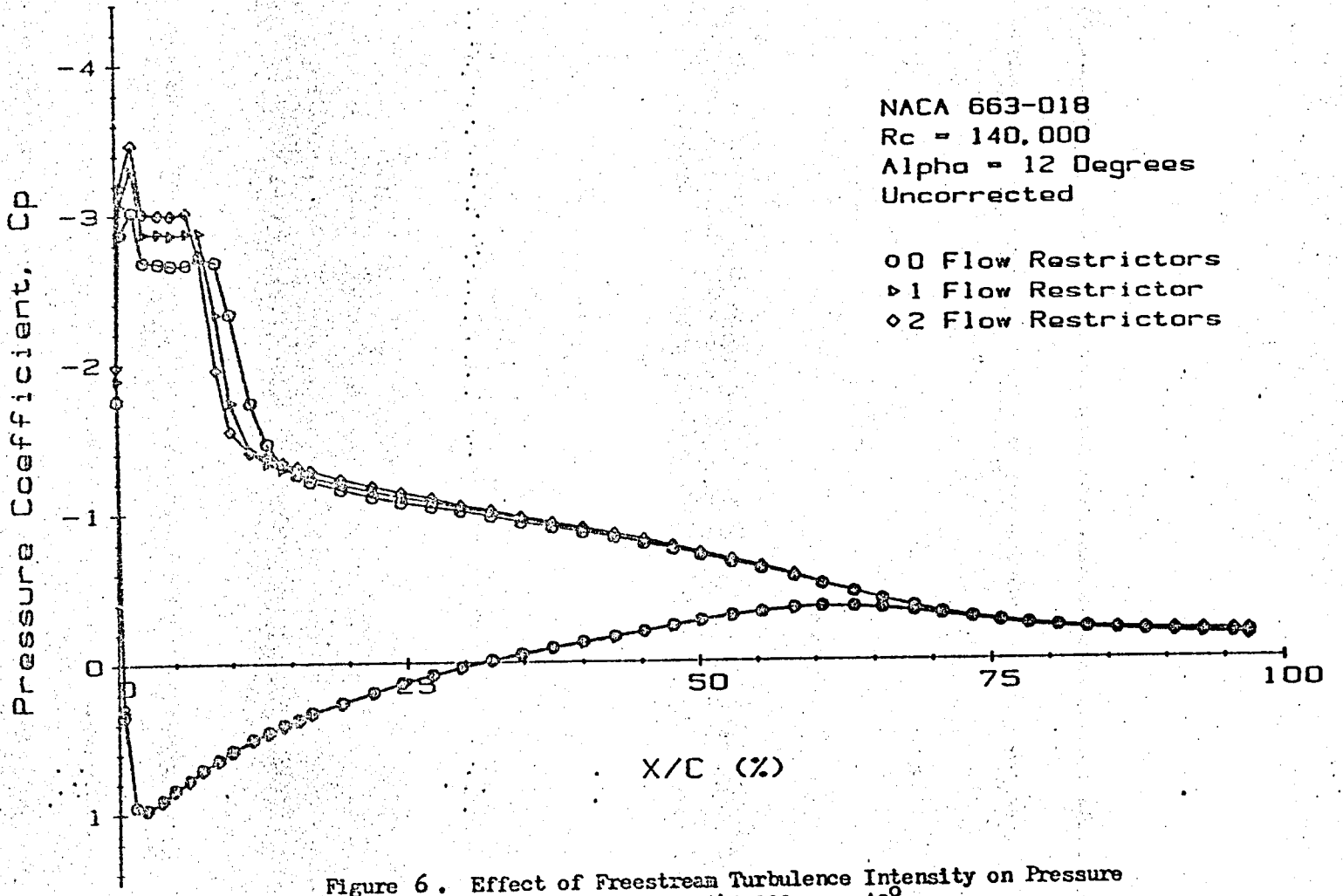

Figure 6. Effect of Freestream Turbulence Intensity on Pressure Distribution, Rc = 140,000, $\alpha = 12^{\circ}$

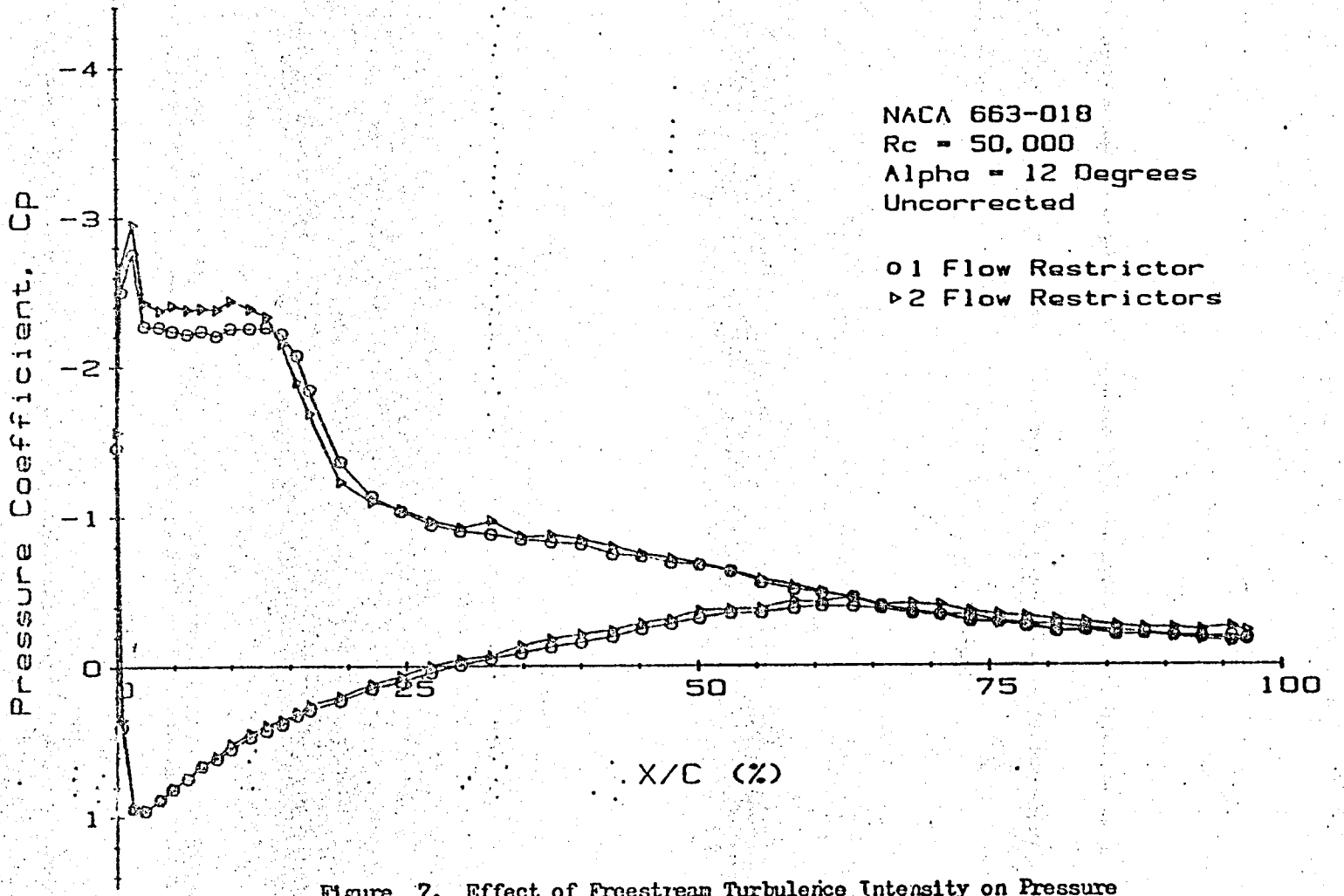

Figure 7. Effect of Freestream Turbulence Intensity on Pressure Distribution, Rc = 50,000, α = 12°

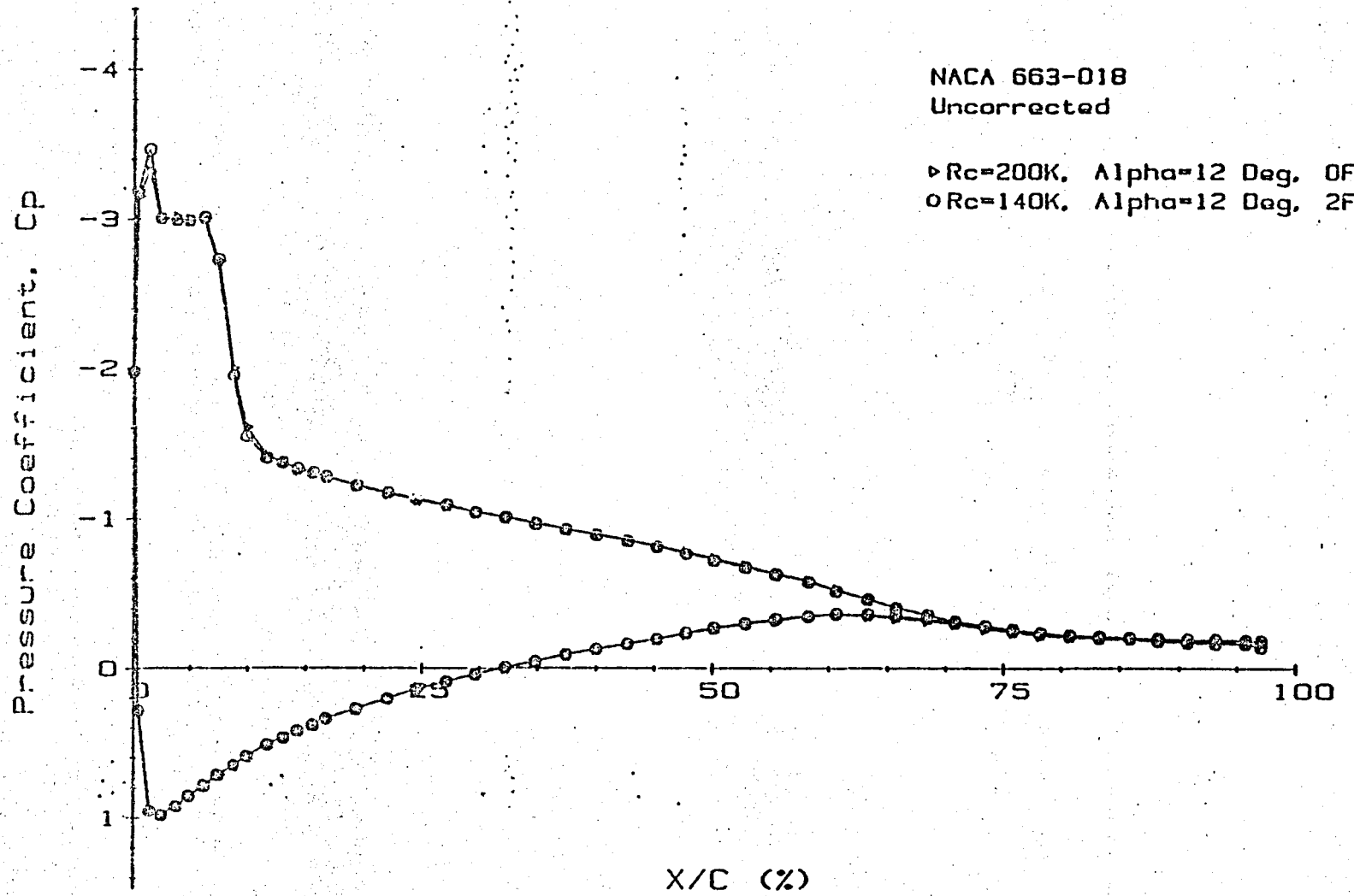

Figure 8. Correlation Between Freestream Turbulence Intensity Increases and Chord Reynolds Number Increases

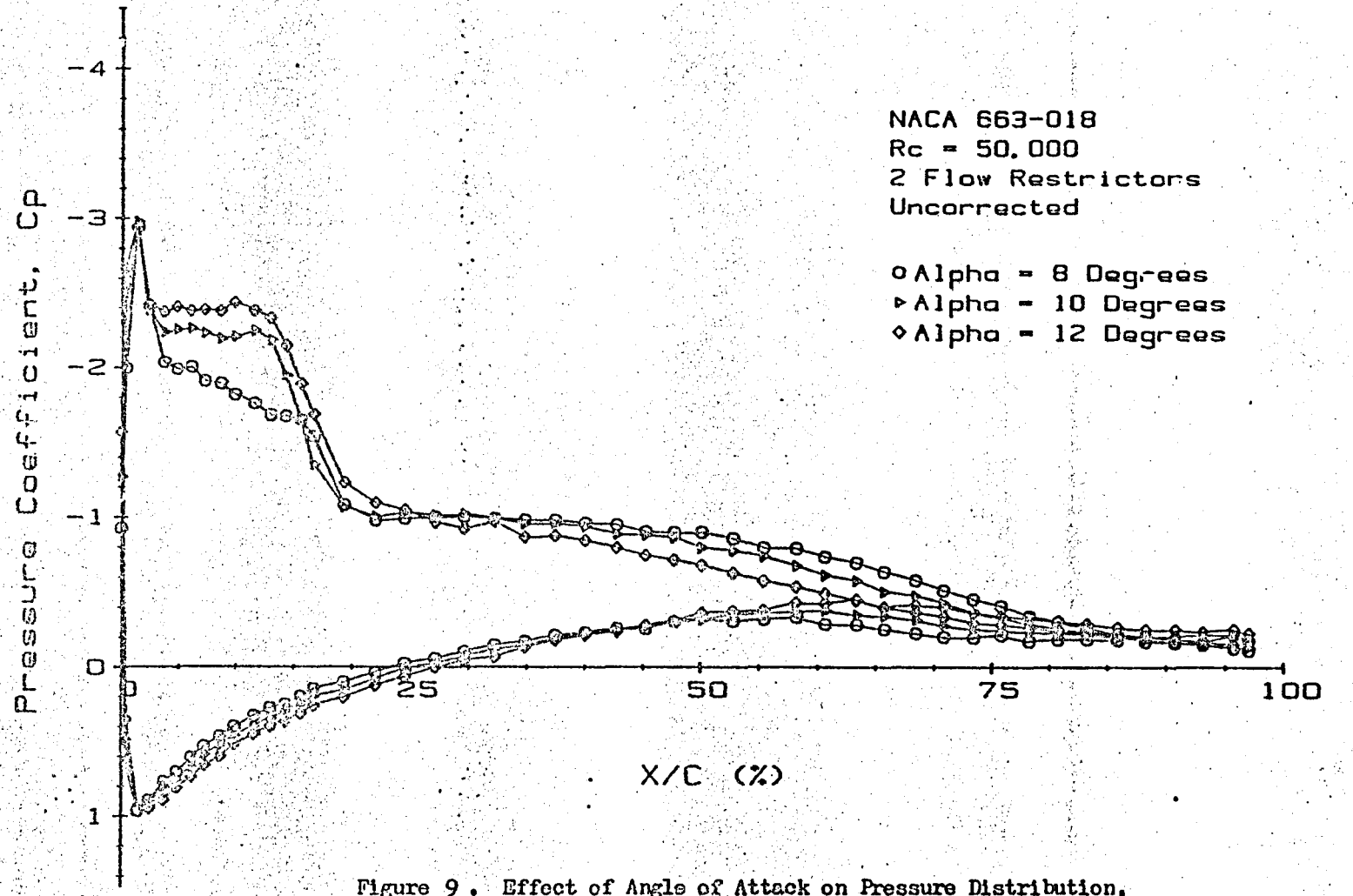

Figure 9. Effect of Angle of Attack on Pressure Distribution, Rc = 50,000, 2 Flow Restrictors

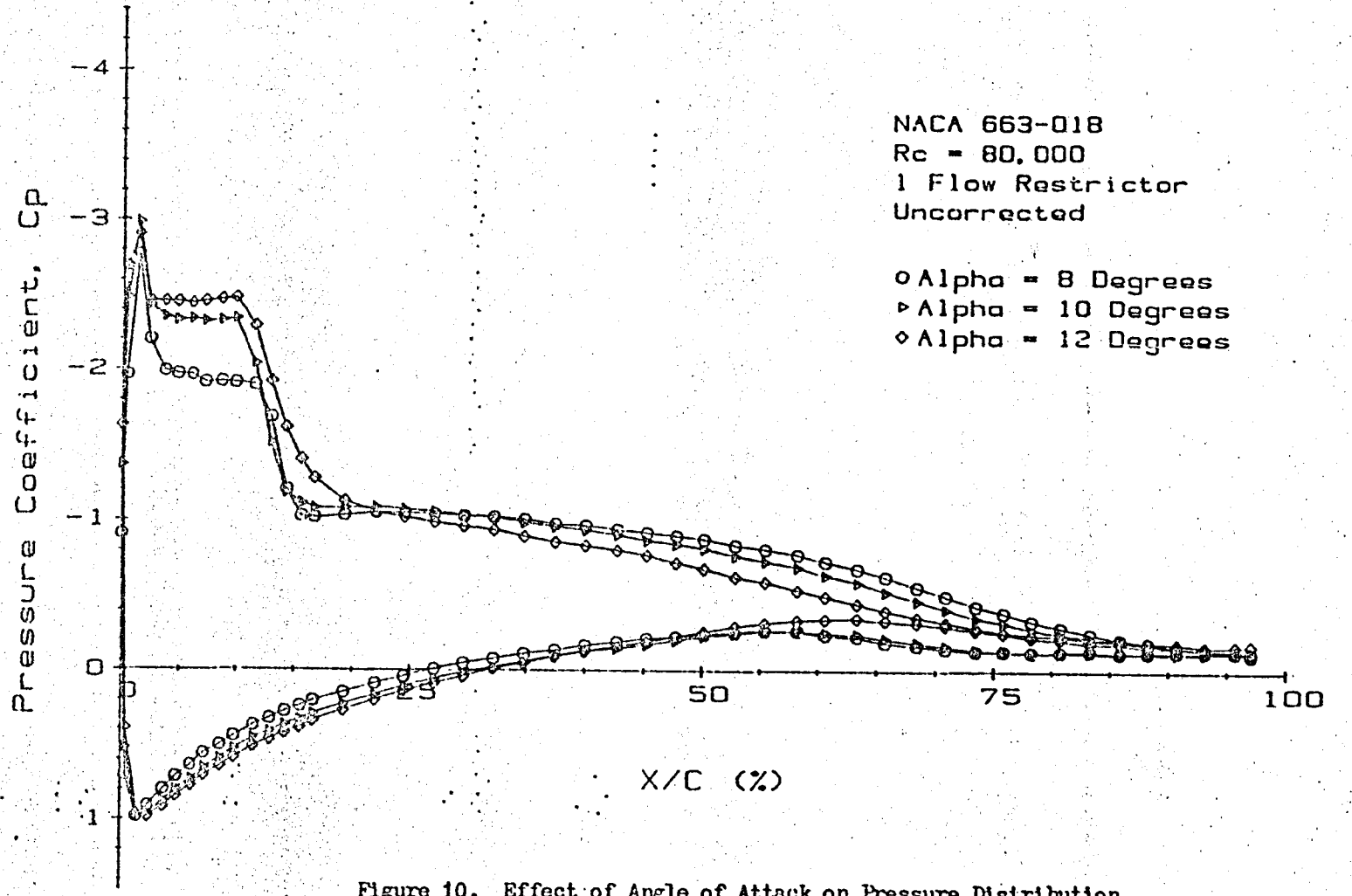

Figure 10. Effect of Angle of Attack on Pressure Distribution, Rc = 80,000, 1 Flow Restrictor

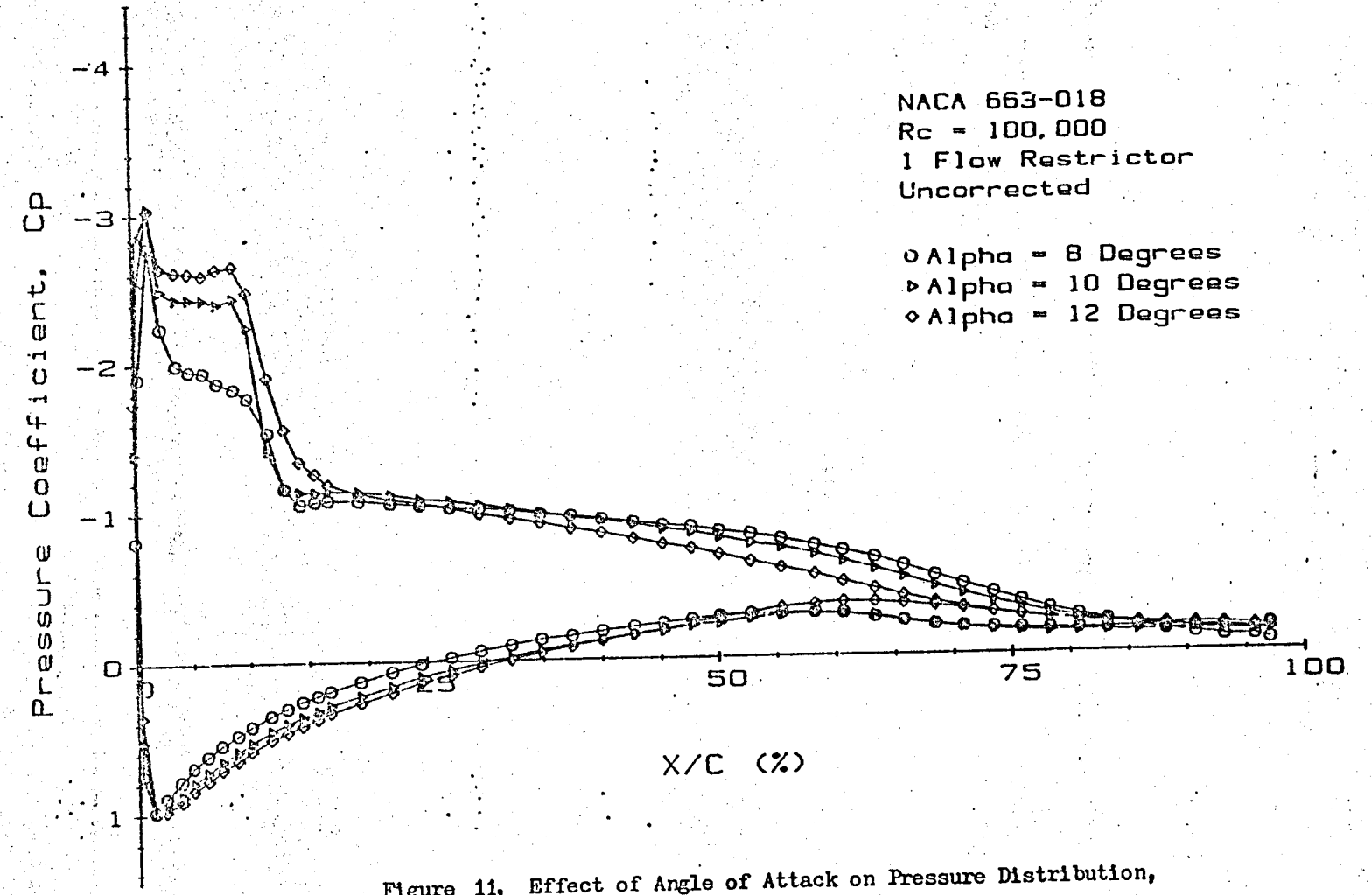

Figure 11. Effect of Angle of Attack on Pressure Distribution, Rc = 100,000, 1 Flow Restrictor

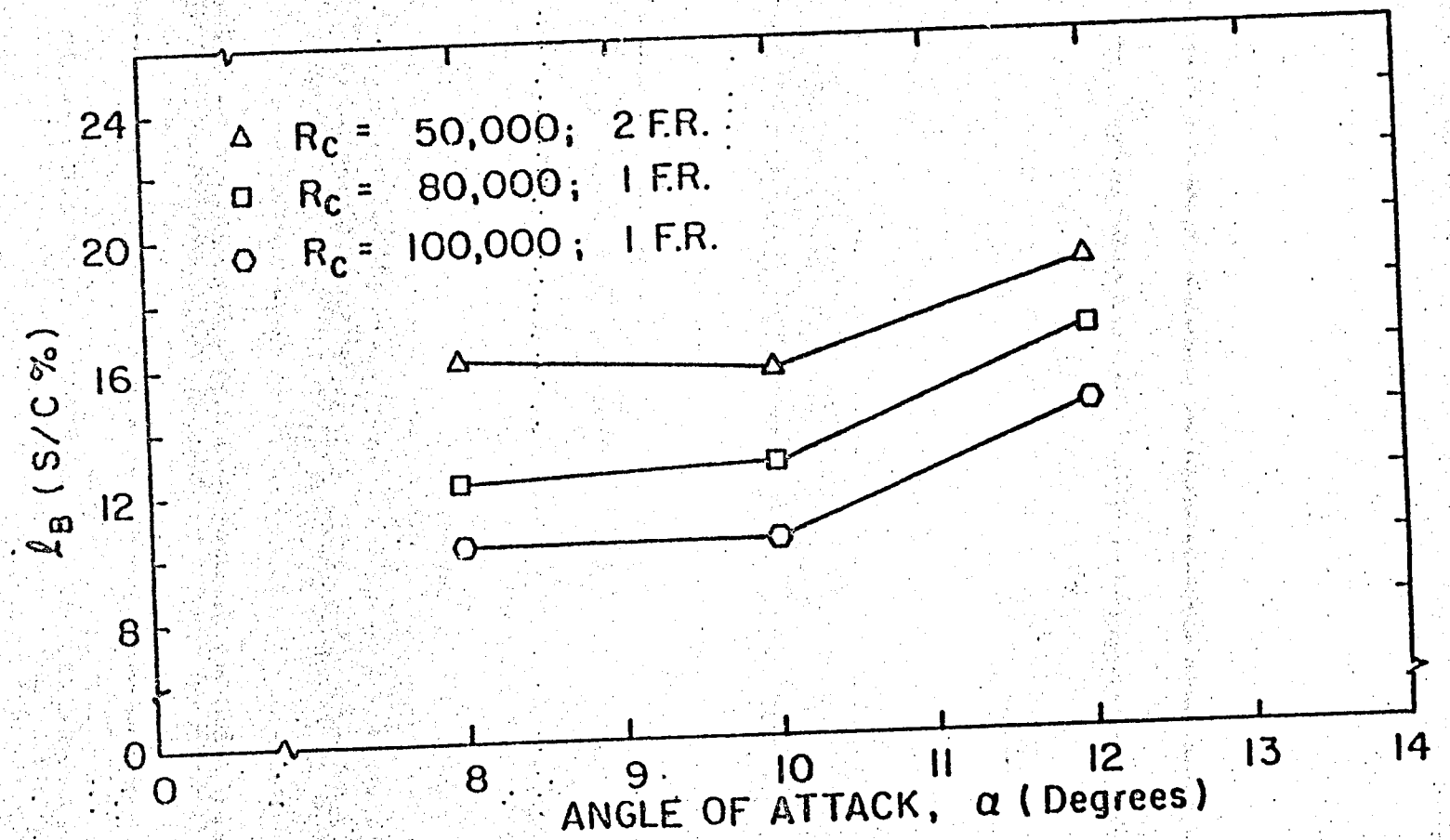

Figure 12. Total Bubble Length versus Angle of Attack

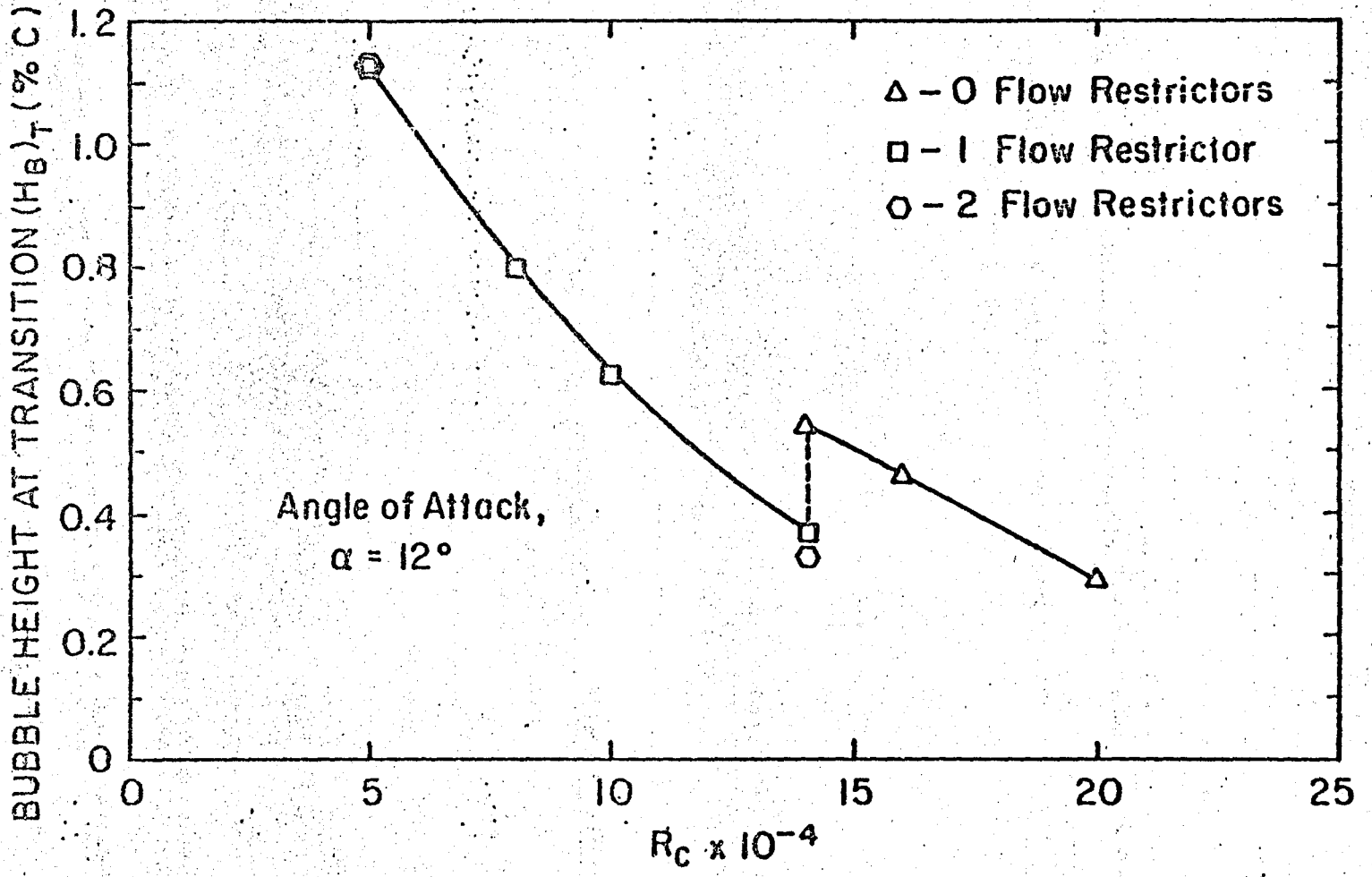

Figure 13. Bubble Height at Transition versus Chord Reynolds Number

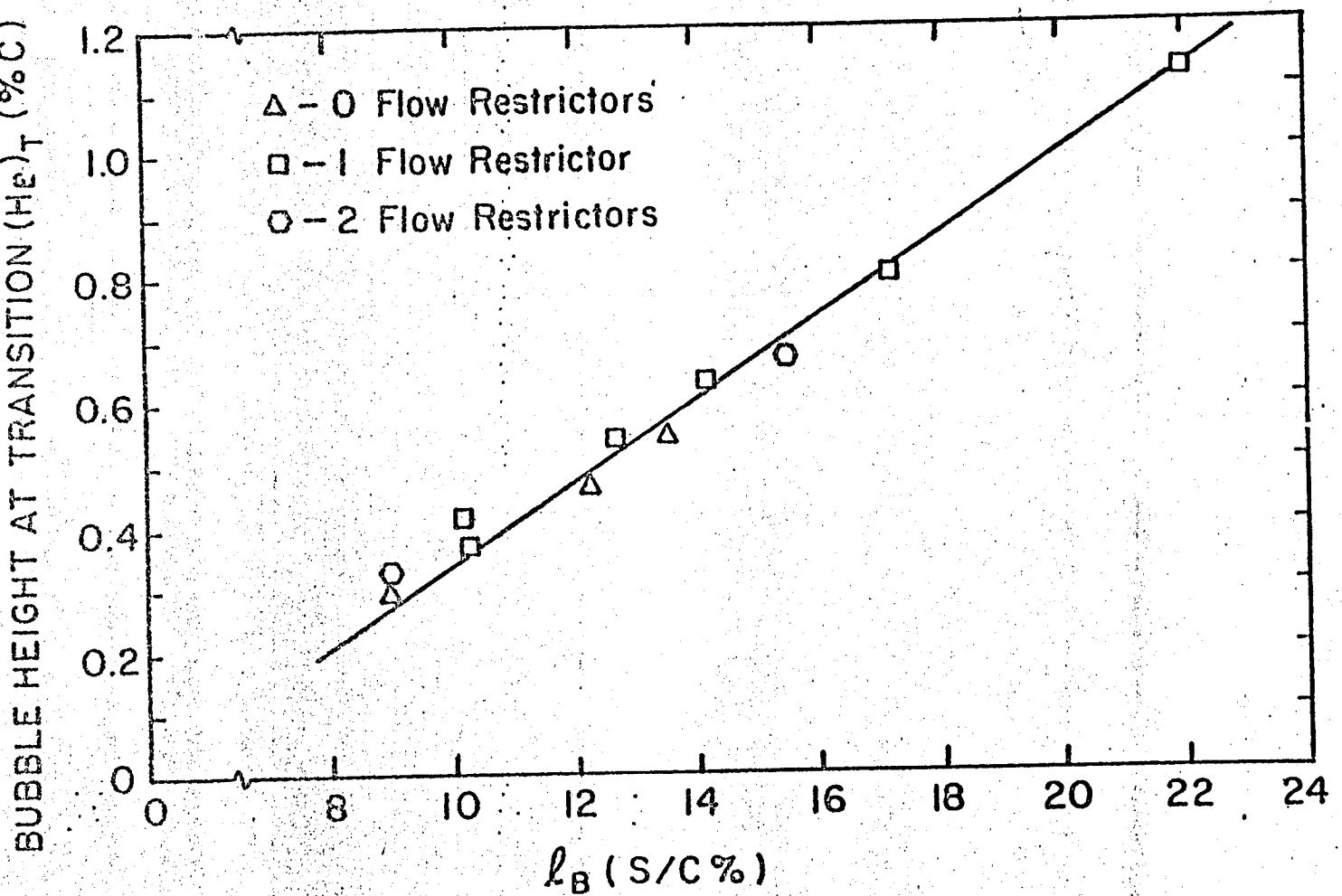

Figure 14. Bubble Height at Transition versus Total Bubble Length

END

DATE

FILMED

JUN 24 198

End of Document